

Oscillation Characteristics Analysis and Equivalent Modeling of Multiple CIGs Connected to Weak Grid

Longyuan Li, Ruiqing Fu, Xiaoqin Lyu, and Xiaoru Wang, *Senior Member, IEEE*

Abstract—The stability problem of weak grid connected converter interfaced generation (CIG) cannot be ignored. For multiple weak grid connected CIGs with different parameters, the system oscillation characteristics and equivalence methods still need to be further studied. This paper first discusses the oscillation characteristics when CIGs are perfectly coupled, perfectly decoupled and their general conditions respectively. Based on the Monte Carlo simulation, the number of critical eigenvalues, the participation of each CIG to critical eigenvalues and the correlative parameters to participation are analyzed. Then the single-CIG and multi-CIG equivalence methods are proposed for stations containing nonidentical CIGs. The CIG parameters of a single-CIG equivalent model are identified based on the consistency of the output admittance characteristics. According to the different participations of CIGs with critical eigenvalues, the station is equivalent to a multi-CIG model. Results of large simulation samples show that the two equivalent models can both preserve the critical eigenvalues very well, and can be used for stability analysis. Furthermore, the multi-CIG equivalent model can also very well reflect the participation of CIGs in detailed models, and can be used for damping control study.

Index Terms—Critical eigenvalues, equivalence, Monte Carlo simulation, multiple CIGs, participation, weak grid.

I. INTRODUCTION

IN order to meet the growing demand for large-scale renewable energy generation, a large number of inverters are being widely used in modern power systems. Converter interfaced generations (CIGs), such as photovoltaic and wind power, are connected to the grid via voltage-source converters. The stable operation of the system with multiple CIGs is very important to the security of power systems.

When CIGs are connected to a weak grid, the control of CIGs can result in cross couplings with dynamics of CIGs and the network, which may lead to unstable power system oscillations over a wide frequency range. Instability phenomena showing relatively low frequencies are classified as slow-interaction converter-driven stability (typically, less

than 10 Hz), while phenomena with relatively high frequencies are classified as fast-interaction converter-driven stability (typically, tens to hundreds of Hz, and possibly into kHz) [1], [2]. This paper focuses on the slow-interaction converter-driven stability. In recent years, there are many reports of oscillation accidents caused by CIGs, such as the type IV wind farm oscillation in China in 2015 and the offshore type IV wind farm oscillation in the UK in 2019 [3]. Researches have shown that the phase locked loop (PLL), DC voltage control (DVC), and AC voltage control (AVC) of CIG are highly correlated with the slow-interaction stability, while inner current control, and even switching control of CIG are largely irrelevant due to the small timescale [1], [4]. Much research about stability of single weak grids connected to CIGs have been studied and many valuable conclusions have been obtained [4]–[7]. However, there are still few studies on multiple CIG systems, especially when the CIGs are not identical [8].

A symmetric system is a special multiple machine system, in which all machines are identical, and the connected-grid impedance is symmetric. It was first studied in the torsional oscillation of synchronous generation [9], [10]. In recent years, researchers have extended it to the system of multiple weak grid connected CIGs [11], [12]. Their research shows that: A symmetric system with n CIG will have a set of eigenvalues, which is observable both on the CIGs side and the grid side. The eigenvectors to the eigenvalues of each CIG are exactly the same, thus it is called an in-phase mode in the torsional oscillation. Meanwhile, the system has another $n-1$ set of eigenvalues, which are only observable at the CIGs side, but not at the grid side. Therefore, the CIGs oscillate with each other, which are called anti-phase modes [9]–[12]. The above conclusions can be derived from matrix theory and can be strictly proved. The same conclusion was drawn for all similar symmetric systems, for example, the high-frequency stability problem in [13].

Equivalence is necessary in multiple CIG systems analysis due to large-scale model and dimensionality disaster. For symmetric CIG systems, normally, the in-phase mode will be always weaker than the anti-phase mode, and the grid does not participate in the anti-phase mode. Therefore, only the in-phase mode needs to be considered in the equivalence [10]–[12]. Through matrix transformation, the detailed system is transformed into n independent subsystems. The subsystem related to the in-phase mode is taken as the single-CIG equivalent model, which are the equivalence ideas in [10]–

Manuscript received February 3, 2021; revised August 10, 2021; accepted September 7, 2021. Date of online publication May 6, 2022; date of current version October 19, 2022. This work was supported by the Applied Basic Research Program of Science and Technology Plan Project of Sichuan Province of China (No. 2020YJ0252).

L. Y. Li, R. Q. Fu, X. Q. Lyu, and X. R. Wang (corresponding author, email: xrwang@home.swjtu.edu.cn) are with the School of Electrical Engineering, Southwest Jiaotong University, Chengdu 611756, China.

DOI: 10.17775/CSEEJPES.2021.00910

[12]. The method that the grid impedance multiplies n times in [13] is essentially the same idea. In addition, there are also equivalence methods to preserve the interaction mode (i.e., anti-phase) between CIGs. Ref. [14] introduces double machines equivalence to preserve both in-phase mode and anti-phase mode.

Furthermore, some research has been carried out based on some special asymmetric systems, which are the symmetric system with less strict assumptions. In [15], [16], the system with identical machines and asymmetric grid impedance is studied. In [17], the system, that all wind turbine generators have approximated open-loop modes, is studied. Considering the asymmetric collector lines in wind farms, the wind farm is equivalent to a single machine model based on matrix transformation [16].

For an asymmetric system, which is more generally, current research primarily focuses on the interactions between each of the CIGs [18]–[20]. However, for the oscillation characteristics of the whole system, there are still few studies, which also applies to the equivalence method of the asymmetric CIG system. Ref. [21] proposes a dynamic aggregation modeling method of CIGs using coherency-based equivalence. But the aggregation method is based on the premise of DC voltage having coherency, which has some limitations in applications.

Various research shows that when the multiple weak grid connected CIGs are in a symmetric system, only one pair of critical eigenvalues (in-phase mode) needs to be focused on [10]–[12]. However, in the asymmetric system of CIGs, the default assumption that the system has only one pair of critical eigenvalues is taken [22]. Whether this assumption is correct remains to be verified. On the other hand, in the symmetric system, CIGs have the same eigenvectors and participation factors to the critical eigenvalues (in-phase mode). On the contrary, because of not having identical CIGs in the asymmetric system, the participation of CIGs with the critical eigenvalues are different. But which parameters the participation is related to still needs to be explored.

When studying the stability of large-scale weak grid connected CIGs, if modeling all CIGs in each station, it will bring about a large number of problems, such as big workload, dimension disaster, poor calculation speed and convergence. Therefore, it is necessary to study the equivalent model of CIG stations within the premise of preserving the critical eigenvalues. It will reduce the analysis complexity and ensure accuracy. When analyzing stability of the symmetric CIG systems, it can be equivalent to a single-CIG model [10]–[12]. But in the asymmetric of the CIG system, the single-CIG equivalence is possible only if the system has only one pair of critical eigenvalues. The single-CIG equivalent model is very concise, but it cannot distinguish the differences of all CIGs. For example, when applying damping control, the CIGs with higher participation should be identified as the candidate locations. At this time, the system should be equivalent to the multi-CIG model.

The contributions in this paper are as follows. First, the oscillation characteristics of multiple weak grid connected CIGs with different parameters are analyzed. It is found that the system may have multiple critical eigenvalues which

depends on the coupling degree of CIGs. The participation of CIG to the critical eigenvalues is primarily related to the PLL bandwidth and the coupling degree of CIGs. Secondly, based on the oscillation characteristics of the system, the single-CIG and multi-CIG equivalence methods for CIG stations are proposed, which can be applied to stability analysis and damping control studies respectively.

The remainder of this paper is organized as follows. Section II presents the CIG model. The oscillation characteristics of multiple weak grid connected CIGs in an asymmetric system are analyzed in Section III. The single-CIG and multi-CIG equivalence methods are proposed respectively in Section IV. Section V provides a simulation example. The conclusion is presented in Section VI.

II. CIG MODEL

The oscillation of a weak grid connected CIG is primarily related to the grid-side converter and its control. Therefore, the generator side of CIG is ignored and is equivalent to a power source. In practical applications, most onshore type IV wind turbine generators and photovoltaic powers use two-level converters [23], [24]. Refs. [4]–[7] also use a two-level converter model to study the single weak grid connected CIG systems. Therefore, the two-level converter model is also adopted as a CIG model in the multiple weak grid connected CIG system in this paper, and the other topologies, such as a modular multilevel converter, are not considered. The established CIG model consists of DVC (2nd order), PLL (2nd order), AVC (1st order), and current control (4th order), as shown in Fig. 1.

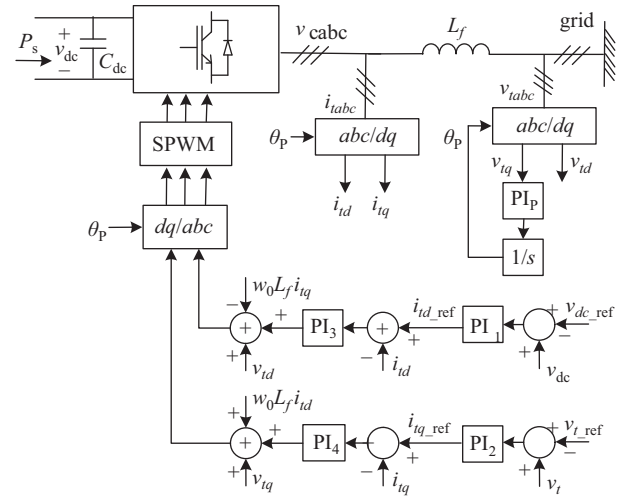


Fig. 1. CIG model.

The CIG small signal model has been derived in many papers [4]–[7]. This paper only gives the state space modeling and impedance modeling results. The state space model is as follows.

$$\begin{cases} \Delta \dot{x}_W = A_{WW} \Delta x_W + A_{WV} \Delta x_V \\ \Delta i_W = C_W \Delta x_W \end{cases} \quad (1)$$

where

$$\begin{aligned}\Delta \mathbf{x}_W &= [\Delta x_P \ \Delta \theta_P \ \Delta v_{dc} \ \Delta x_1 \\ &\quad \Delta x_2 \ \Delta x_3 \ \Delta x_4 \ \Delta i_{td} \ \Delta i_{tq}]^T \\ \Delta \mathbf{x}_V &= [\Delta v_{tx} \ \Delta v_{ty}]^T \\ \Delta \mathbf{i}_W &= [\Delta i_{tx} \ \Delta i_{ty}]^T\end{aligned}$$

are state variables, input variables composed of terminal voltage, and output variables composed of the output current of CIG, respectively. The matrices \mathbf{A}_{WW} , \mathbf{A}_{WV} and \mathbf{C}_W are state matrix ($9^{\text{th}} \times 9^{\text{th}}$ order), input matrix ($9^{\text{th}} \times 2^{\text{nd}}$ order) and output matrix ($2^{\text{nd}} \times 9^{\text{th}}$ order) respectively.

The impedance model is also one of the mainstream models for analyzing the stability of CIG. The impedance model is given as follows.

$$\begin{bmatrix} \Delta i_{tx} \\ \Delta i_{ty} \end{bmatrix} = - \begin{bmatrix} Y_{xx} & Y_{xy} \\ Y_{yx} & Y_{yy} \end{bmatrix} \begin{bmatrix} \Delta v_{tx} \\ \Delta v_{ty} \end{bmatrix} \quad (2)$$

where v_t and i_t are terminal voltage and output current of CIG,

$$\begin{bmatrix} Y_{xx} & Y_{xy} \\ Y_{yx} & Y_{yy} \end{bmatrix} = \begin{bmatrix} \cos \theta_0 & -\sin \theta_0 \\ \sin \theta_0 & \cos \theta_0 \end{bmatrix} \begin{bmatrix} Y_{dd} & Y_{dq} \\ Y_{qd} & Y_{qq} \end{bmatrix} \begin{bmatrix} \cos \theta_0 & \sin \theta_0 \\ -\sin \theta_0 & \cos \theta_0 \end{bmatrix}$$

\mathbf{Y}_{xy} is the admittance in global coordinates; \mathbf{Y}_{dq} is the admittance in local coordinates; θ_0 is the steady-state value of the terminal voltage phase angle in the global coordinate. The expression of each element is as follows:

$$\begin{aligned}Y_{dd} &= G_{dvc}(s) \frac{i_{td0}}{v_{td0}}, \quad Y_{qq} = -G_{pll}(s) G_{ccq}(s) \frac{i_{td0}}{v_{td0}} \\ Y_{dq} &= (G_{dvc}(s) + (1 - G_{dvc}(s)) G_{pll}(s) G_{ccd}(s)) \frac{i_{tq0}}{v_{td0}} \\ Y_{qd} &= -K_{avc}(s) G_{ccq}(s)\end{aligned} \quad (3)$$

where $G_{ccd}(s)$, $G_{ccq}(s)$, $G_{dvc}(s)$, $G_{pll}(s)$ are the transfer function of the d -axis current control, q -axis current control, DVC, PLL respectively; $K_{avc}(s)$ is the transfer function of PI controller of AVC. The expressions are as follows:

$$\begin{aligned}G_{ccd}(s) &= \frac{s \frac{K_{p3}}{L_f} + \frac{K_{i3}}{L_f}}{s^2 + s \frac{K_{p3}}{L_f} + \frac{K_{i3}}{L_f}}, \quad G_{ccq}(s) = \frac{s \frac{K_{p4}}{L_f} + \frac{K_{i4}}{L_f}}{s^2 + s \frac{K_{p4}}{L_f} + \frac{K_{i4}}{L_f}} \\ G_{dvc}(s) &= \frac{\left(s \frac{K_{p1} v_{td0}}{C v_{dc0}} + \frac{K_{i1} v_{td0}}{C v_{dc0}} \right) G_{ccd}(s)}{s^2 + \left(s \frac{K_{p1} v_{td0}}{C v_{dc0}} + \frac{K_{i1} v_{td0}}{C v_{dc0}} \right) G_{ccd}(s)} \\ G_{pll}(s) &= \frac{s K_{pP} v_{td0} + K_{iP} v_{td0}}{s^2 + s K_{pP} v_{td0} + K_{iP} v_{td0}} \\ K_{avc}(s) &= K_{p2} + \frac{K_{i2}}{s}\end{aligned} \quad (4)$$

III. OSCILLATION CHARACTERISTICS ANALYSIS OF MULTIPLE WEAK GRID CONNECTED CIGS IN ASYMMETRIC SYSTEM

This section primarily answers the following two questions by analyzing the oscillation characteristics of multiple weak grid connected CIGs in an asymmetric system. 1) How many pairs of critical eigenvalues does the system have? 2) How

much does each CIG participate in the critical eigenvalues? And which parameters is the participation related to? There are different answers for different scenarios.

A. The Multiple CIG System

The asymmetric system studied in this section is: the output and parameters of each CIG are not exactly the same, or the grid structure is asymmetrical. By using Kron reduction [25] to eliminate all interior nodes, the system can be equivalent to the figure on the left of Fig. 2. Since all systems can be reduced to the following standard form by Kron reduction, the analysis is based on this standard system.

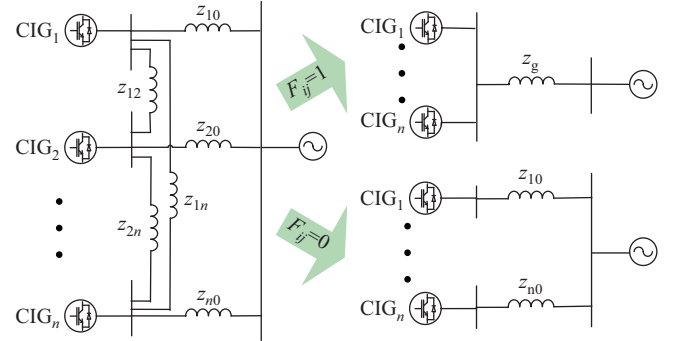


Fig. 2. Multiple CIGs connection diagram.

The multi-infeed interaction factor is introduced to relate interaction between any two inverter AC voltages. It is used in estimating the degree of voltage interaction between two HVDC systems. The multi-infeed interaction factor from inverter i AC bus to inverter j AC bus is defined by (5) and is essentially a measure of the impact that a 1% voltage drop (ΔV_i) at the inverter i AC bus has on the line voltage at inverter j [26]. It is deduced that $MIIF_{ji}$ is equal to the ratio of mutual-impedance Z_{ji} and self-impedance Z_{ii} [27].

$$MIIF_{ji} = \frac{\Delta V_j}{\Delta V_i} = \frac{Z_{ji}}{Z_{ii}} \quad (5)$$

The multi-infeed interaction factor is asymmetric, i.e., $MIIF_{ji} \neq MIIF_{ij}$. It can be obtained by these two methods.

a) The voltage drop test [26]. An about 1% voltage drop ΔV_i is applied at the CIG i , and the voltage drop at the CIG j ΔV_j can be measured. The ratio of the two voltage drops is $MIIF_{ji}$.

b) The ratio of mutual-impedance and self-impedance [27]. In practical terms, mutual-impedances and self-impedances are not easy to be obtained directly. Fortunately, they can be obtained based on the identification method. First, obtain the admittance matrix \mathbf{Y} of the system with only CIG nodes based on online identification [28]. Then calculate the impedance matrix $\mathbf{Z} = \mathbf{Y}^{-1}$, whose diagonal elements and other elements are self-impedance Z_{ii} and mutual-impedance Z_{ji} respectively. Finally, obtain $MIIF_{ji} = Z_{ji}/Z_{ii}$.

Based on the multi-infeed interaction factor, the coupling degree index between CIG i and CIG j is defined as the average value of $MIIF_{ji}$ and $MIIF_{ij}$.

$$F_{ij} = F_{ji} = \frac{1}{2} (MIIF_{ij} + MIIF_{ji}) \quad (6)$$

The coupling degree index meets $0 \leq F_{ij} \leq 1$. The larger F_{ij} , the greater the coupling degree between the two CIGs. When $F_{ij} = 1$, the two CIGs are perfectly coupled, and when $F_{ij} = 0$, the two CIGs are perfectly decoupled.

According to the coupling degree of CIGs, the system is divided into three scenarios. The first one is that all CIGs are perfectly coupled (i.e., $F_{ij} = 1$, all CIGs are parallel on the same bus, as shown on the upper right of Fig. 2). The second one is that all CIGs are perfectly decoupled (i.e., $F_{ij} = 0$, all CIGs are separately connected to the infinite system, as shown on the lower right of Fig. 2). The last one is the general system, as shown on the left of Fig. 2. The oscillation characteristics of these three systems are analyzed in Parts B, C, and D.

B. System with Multiple Perfectly Coupled CIGs

Due to the different parameters of each CIG, and the large number of CIGs, it is difficult to analyze theoretically. Therefore, the Monte Carlo method is adopted in this section to analyze oscillation characteristics through large-scale simulation samples.

1) Critical Eigenvalues Analysis

The critical eigenvalues refer to the negative damped or weak damped eigenvalues. In this paper, the threshold is set as the damping ratio, which is less than 0.05.

For the system with $n = 66$ parallel CIGs connected to the weak grid (as shown on the upper right of Fig. 2), the Monte Carlo simulation is designed as follows:

Step 1: Randomly generate the parameters of every CIG, include output power, bandwidth and damping of DVC and PLL, and the PI controller parameters of AVC. The parameters are different between each CIG. To avoid unpractical situations, such as lower damping of PLL, the parameters of each CIG should be within the normal range. The upper and lower limits of CIG parameters are given in Table I.

TABLE I
UPPER AND LOWER LIMITS OF CIG PARAMETERS

CIG parameters	Lower limits	Upper limits
PLL bandwidth (Hz)	10	40
PLL damping	0.30	0.80
DVC bandwidth (Hz)	5	25
DVC damping	0.30	0.80
AVC proportional coefficient (S)	0.2	20
AVC integral coefficient (S/s)	8	800
Output power (p.u.)	0.05	1

Step 2: Obtain the state matrix of the system, and calculate the eigenvalues.

Step 3: Analyze the characteristics of critical eigenvalues.

$N = 2000$ random samples are used to calculate and analyze. The results show that there are only one pair of critical eigenvalues in every sample. A typical eigenvalue distribution is shown in Fig. 3. Only one pair of eigenvalues is negative damped, while the rest are strong damped. The eigenvalue distributions in all samples are similar to Fig. 3. Large sample statistical analysis shows that the number of critical eigenvalues is not related to the random parameters. After repeating the simulation 2000 times there is still only one pair of critical eigenvalues.

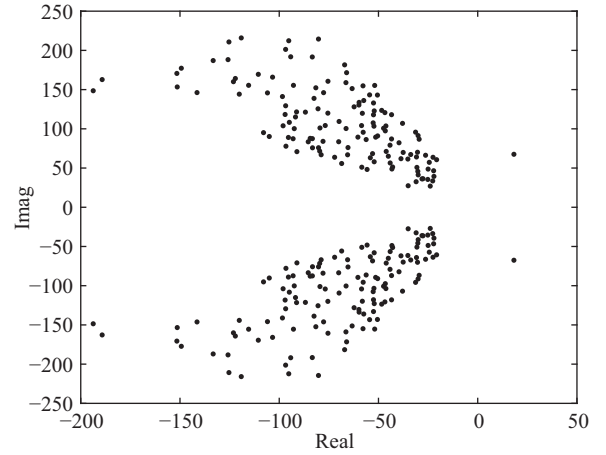


Fig. 3. A typical eigenvalues scatter diagram.

Calculate the difference between the damping ratio of the weakest eigenvalues and the second weakest eigenvalues, and obtain the maximum, minimum and average values of the differences of the damping ratio in all samples, which is the first column of Table II. The results of the real part are obtained by the same method, i.e., the second column of Table II. As can be seen from the first column, the damping of critical eigenvalues is on average 0.5853 weaker than that of other eigenvalues. As shown in the second column, the critical eigenvalues are on average 30.0128 more right than other eigenvalues. Both the damping ratio and the real part indicate that the critical eigenvalues (weakest eigenvalues) are significantly weaker than other eigenvalues. It shows that the oscillation mode corresponding to non-critical eigenvalues attenuate rapidly because of the strong damping, and the modes are difficult to be observed in the system. However, the oscillation mode corresponding to the critical eigenvalues attenuates slowly even increasing due to its weak damping, and it is easy to be observed.

TABLE II
COMPARISON OF THE WEAKEST AND SECOND WEAKEST EIGENVALUES

Statistical items	Difference of damping ratio	Difference of real part
Average value	-0.5853	30.0128
Maximum value	-0.7662	50.8938
Minimum value	-0.3386	18.5668

In the symmetric multiple CIG systems, both CIGs and grid participated in the critical eigenvalues (i.e., in-phase mode), while only CIGs participated in the non-critical eigenvalues (i.e., anti-phase mode) [9]–[12]. Now the participation of CIGs and grid to the different eigenvalues in the asymmetric multiple CIG system will be studied.

Based on the small signal state space model, the eigenvalue analysis method is used to obtain the eigenvalue λ and its right eigenvector φ and left eigenvector ψ of the system. Let p_{rs} denote the participation factor of the r^{th} state variable x_r to the s^{th} eigenvalue λ_s , defined as:

$$p_{rs} = \varphi_{rs} \psi_{rs} \quad (7)$$

where φ_{rs} is the r^{th} row of the right eigenvector φ_s ; ψ_{rs} is the r^{th} row of the left eigenvector ψ_s .

Based on the participation factor, the relative participations of all CIGs and grid are defined as follows [29]:

$$\begin{aligned}\sigma_{\text{CIGs},s} &= \sum_{k=1}^n \|\rho_{ks}\|_1 / \sum_{k=1}^{n+1} \|\rho_{ks}\|_1 \\ \sigma_{\text{grid},s} &= \|\rho_{n+1,s}\|_1 / \sum_{k=1}^{n+1} \|\rho_{ks}\|_1\end{aligned}\quad (8)$$

where $\|\cdot\|_1$ is l_1 -norm; $\sigma_{\text{CIGs},s}$ and $\sigma_{\text{grid},s}$ are the relative participation of the all CIGs and grid to the s^{th} eigenvalue respectively; ρ_{ks} ($k = 1, 2, \dots, n$) is a vector composed of the participating factors (as shown in (7)) of all state variables of the k^{th} CIG to the s^{th} eigenvalue; $\rho_{n+1,s}$ is a vector composed of the participating factors of all state variables of the grid to the s^{th} eigenvalue. The relative participation of σ can intuitively indicate the participation of all CIGs or grid to the eigenvalues. The higher σ is, the greater the participation of CIGs or grid.

Based on (8), the σ_{CIGs} and σ_{grid} to all eigenvalues in all samples can be calculated. In all $N = 2000$ samples, the average values of σ_{CIGs} and σ_{grid} to the critical and non-critical eigenvalues can be obtained, as shown in Table III. The statistical results show that both CIGs and grid participated in the critical eigenvalues, and the grid has almost no participation in non-critical eigenvalues. This means that the grid has great observability and controllability only for the critical eigenvalues, but poor observability and controllability for other eigenvalues.

TABLE III
AVERAGE VALUES OF RELATIVE PARTICIPATIONS OF ALL
CIGS AND GRID

Statistical items	Critical eigenvalues	Non-critical eigenvalues
σ_{CIGs}	0.7997	0.9970
σ_{grid}	0.2003	0.0030

The CIG station is a subset of the multiple CIG systems studied in this section. In the above case study, the Monte Carlo method is used for general multiple CIG systems which could consist of several CIG stations and the parameters among the different types of CIGs have a wide range of randomness. Therefore, each CIG is simulated to have individual parameters and a total of 66 sets of CIG parameters are set up in the sampling.

In a single CIG station, there may be only a few types of CIGs and the parameters among the same type of CIGs are highly consistent. The Monte Carlo simulations, for a single CIG station scenario, are also studied. The Monte Carlo simulation is designed so that six sets of CIG parameters or two sets of CIG parameters are respectively randomly generated. The statistical analysis of $N = 2000$ samples for each case shows that the system still has only one pair of critical eigenvalues, which is consistent with the previous conclusion.

In summary, when the CIGs are perfectly coupled and connected into the grid, the system has only one pair of critical

eigenvalues. The grid has a large participation only in critical eigenvalues, but almost no participation in other eigenvalues.

2) Participation Analysis

In order to analyze the participation of each CIG in the critical eigenvalues, the concept of relative participation is introduced. The details are as follows.

Based on the participation factor, the relative participation of each CIG to the critical eigenvalues is defined as follows [29]:

$$\eta_k = \|\rho_k\|_1 / \sum_{j=1}^n \|\rho_j\|_1 \quad (9)$$

where $\|\cdot\|_1$ is l_1 -norm; n is the number of CIGs; η_k is the relative participation of the k^{th} CIG; ρ_k is a vector composed of the participating factors (as shown in (7)) of all state variables of the k^{th} CIG to critical eigenvalues. Relative participation η_k can intuitively indicate the participation of k^{th} CIG to critical eigenvalues in all CIGs. Among all CIGs, the higher η_k is, the greater the participation of k^{th} CIG to the critical eigenvalues.

Based on the Monte Carlo simulation, the relative participation $\eta_1 \sim \eta_n$ of each CIG in all samples can be obtained. Starting from the first sample, the n scattered points are successively drawn, the two coordinates of which are relative participation and PLL bandwidth of the CIG. All N samples are drawn on a graph, which is Fig. 4(a). Scatter diagrams of other parameters can be plotted in the same way. Some scatter diagrams are shown in Fig. 4.

It can be seen that the lower the PLL bandwidth, the greater the relative participation of the CIG. There is a significant negative correlation between them. DVC bandwidth is also negative correlated with relative participation, but the correlation is not as strong as the PLL bandwidth. In addition, there is little correlation between the output power and relative participation.

In order to quantitatively study the correlation, the Pearson correlation coefficient is introduced as follows:

$$r_{X,Y} = \frac{\sum_{i=1}^m (X_i - \bar{X})(Y_i - \bar{Y})}{\sqrt{\sum_{i=1}^m (X_i - \bar{X})^2} \sqrt{\sum_{i=1}^m (Y_i - \bar{Y})^2}} \quad (10)$$

where, X and Y are two variables. The value of r is between -1 and 1 . Positive value means positive correlation; negative value means negative correlation; and 0 means linearly independent. In general, r between 0.8 – 1.0 indicates a very strong correlation; 0.6 – 0.8 a strong correlation; 0.4 – 0.6 a moderate correlation; 0.2 – 0.4 a weak correlation; 0 – 0.2 a very weak correlation or no correlation. In the calculation of the correlation coefficient, the significance test is also required. Generally, significance level $P < 0.05$ is considered to be relatively significant.

The correlation coefficient between each parameter and the relative participation is calculated, and the results are shown in Table IV. It can be seen that only two parameters, PLL bandwidth and DVC bandwidth, are significantly correlated with the relative participation. PLL bandwidth has a strong negative correlation, while DVC bandwidth has a moderate negative correlation. The remaining parameters are very weak relative with the relative participation.

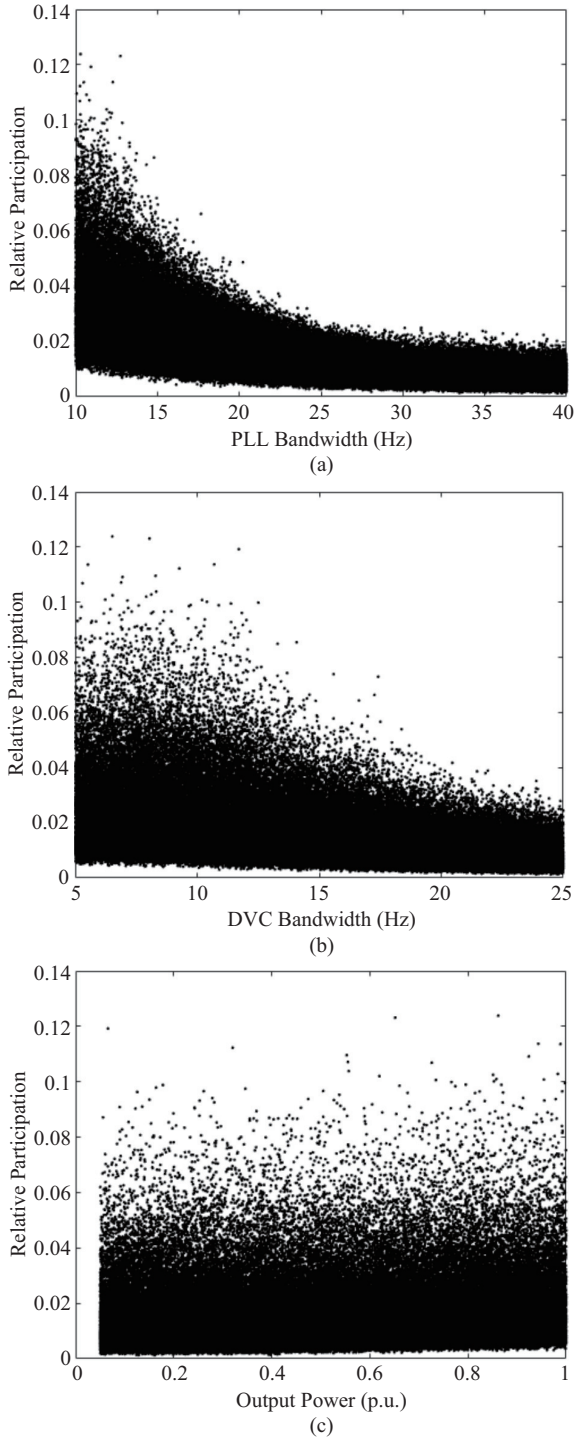


Fig. 4. Scatter diagram of some parameter and relative participation of CIGs. (a) PLL bandwidth and relative participation. (b) DVC bandwidth and relative participation. (c) Output power and relative participation.

A typical diagram of relative participation, PLL bandwidth and DVC bandwidth is shown in Fig. 5. The z -axis is the relative participation of each CIG, the x -axis and y -axis are PLL bandwidth and DVC bandwidth respectively. It is shown that the lower the PLL bandwidth and the lower the DVC bandwidth, the larger the relative participation of CIG. If the DVC bandwidth is high, it is possible that the relative participation of the CIG is still small, even though the PLL

TABLE IV
CORRELATION COEFFICIENT BETWEEN EACH PARAMETER AND THE RELATIVE PARTICIPATION

CIG parameters	Pearson correlation coefficient	Significance level
PLL bandwidth	-0.6661	0
PLL damping	-0.1445	0
DVC bandwidth	-0.4469	0
DVC damping	-0.1694	0
AVC proportional coefficient	0.0031	0.2526
AVC integral coefficient	0.1025	0
Output power	0.1015	0

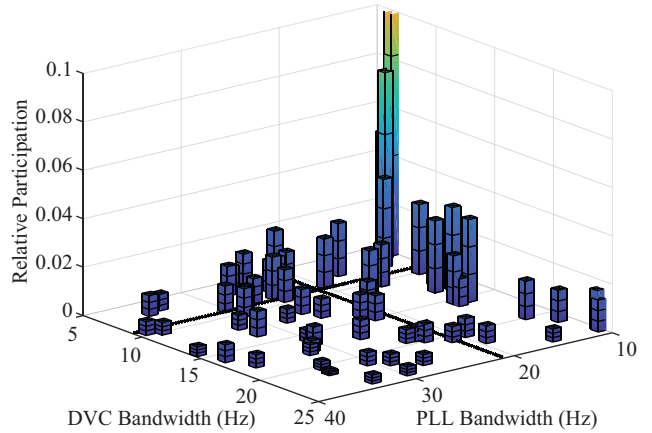


Fig. 5. A typical diagram of relative participation, PLL and DVC bandwidth.

bandwidth is low. However, among the CIGs with similar DVC bandwidth, the law of “the lower the PLL bandwidth, the larger the relative participation” still holds.

C. System with Multiple Perfectly Decoupled CIGs

Obviously, when the CIGs are completely decoupled (as shown on the lower right of Fig. 2), each CIG is independently connected to the infinite bus, which is equivalent to n single CIG systems. In this situation, each system has a pair of critical eigenvalues, and the whole system has n pairs of critical eigenvalues. The eigenvalues of a single CIG system are only related to itself, and have no relationship with other CIGs.

D. General Multiple CIG Systems

According to the analysis of the two special cases above, it can be reasonably inferred that the oscillation characteristics of the general CIG systems are as follows:

The number of critical eigenvalues of the system is related to the coupling degree among each CIG. Obviously, when the coupling degree F_{ij} between the CIGs reduces from 1 to 0, that is, the CIGs change from perfectly coupled to perfectly decoupled, the critical eigenvalues increase from 1 pair to n pairs. Focusing only on the weakest pair of eigenvalues may overlook the potential oscillation risk.

For a pair of critical eigenvalues, as the coupling degree among CIGs decreases, there is definitely a CIG whose participation will gradually increase. When the CIGs are perfectly decoupled, only one CIG participates in the oscillation mode.

It is worth noting that when the connection impedance between each CIG z_{ij} ($i \neq j$) is much smaller than the

connection impedance between each CIG and the power system z_{k0} , the coupling between each CIG is very strong, and the oscillation characteristics of the CIG system are very close to the case of CIGs perfectly coupled.

An example, which is a system with two different CIGs, is used to illustrate the above inference. The coupling degree between the two CIGs is:

$$F_{12} = \frac{1}{2} \left(\frac{z_{20}}{z_{12} + z_{20}} + \frac{z_{10}}{z_{12} + z_{10}} \right) \quad (11)$$

where z_{10} , z_{20} , z_{12} are connection impedance in Fig. 2.

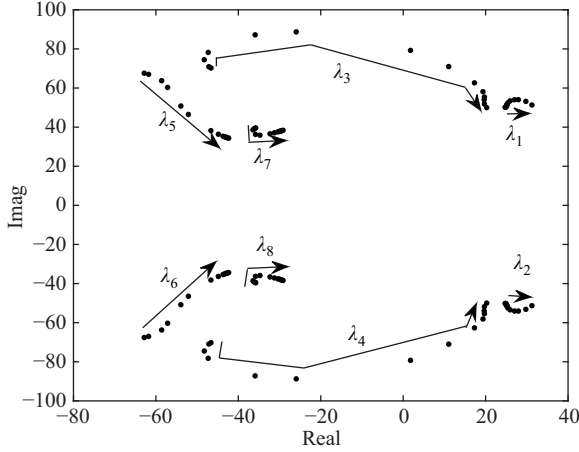


Fig. 6. Eigenvalue trajectories with variable connection impedance.

Let $z_{10} = 103.29$ p.u., $z_{20} = 72.50$ p.u. (in 100 MVA), and z_{12} successively increase from 0 to ∞ (i.e., 0, 1, 5, 10, 50, 100, 500, 1000, 2000, 3000, 4000, 5000, 10000, 10^9). The corresponding case numbers are 1~14). The eigenvalue trajectories with variable connection impedance are shown in Fig. 6. When $z_{12} = 0$, the coupling degree $F_{12} = 1$, there are only one pair of critical eigenvalues $\lambda_{1,2}$. However, with the increase of z_{12} , the coupling degree F_{12} becomes small. The damping of eigenvalues $\lambda_{3,4}$ also becomes negative, and the number of critical eigenvalues becomes two pairs. When the second critical eigenvalue appears (the damping ratio of $\lambda_{3,4}$ is equal to 0.05), the coupling degree of the two CIGs is 0.2011. The relative participations of each CIG to the critical eigenvalues are shown in Fig. 7. The top figure is about eigenvalues $\lambda_{1,2}$, and the bottom figure is about eigenvalues $\lambda_{3,4}$. It can be seen that as the connection impedance z_{12} increases, i.e., the coupling degree F_{12} decreases, the participation of one CIG increases and the participation of the other CIG decreases.

To quantitatively evaluate the relationship between the coupling degree and the number of critical eigenvalues, the simulation of a two-CIG system is designed based on the Monte Carlo method, which is as follows. Randomly generate 2000 sets of samples. The dynamic parameters and output power of two CIGs are within the range of that in Table I. When the connection impedances z_{10} and z_{20} of each sample are constant, the larger the connection impedance z_{12} , the lower the coupling degree between two CIGs. As shown in the previous analysis, when the coupling degree is low enough, the critical eigenvalues will increase from 1 to 2 pairs. When

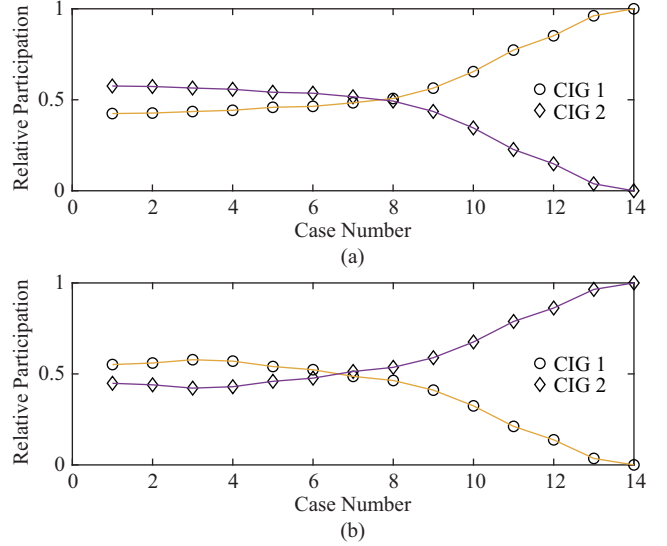


Fig. 7. Relative participations trajectories with variable connection impedance. (a) Relative participation to $\lambda_{1,2}$. (b) Relative participation to $\lambda_{3,4}$.

the second pair of critical eigenvalues appears, the connection impedance z_{12} is calculated. Then the coupling degree index F is calculated by (11). All samples are statistically analyzed, and the results are as follows:

When the second pair of critical eigenvalues appears, the mean value and standard deviation of coupling degree index F of all samples are 0.1432 and 0.1028, respectively. The coupling degree index F in 99% of all samples is below 0.48; in 95% of all samples, it is below 0.33; in 90% of all samples, it is below 0.2775. The results prove the conclusion that when the coupling degree among CIGs is low, the system can indeed have multiple pairs of critical eigenvalues. According to the above results, it is suggested that: when the coupling degree index is less than 0.48, the system is a weak coupled system and may have more than one pair of critical eigenvalues; when the coupling degree index is larger than 0.48, the system is a strongly coupled system and basically has only one pair of critical eigenvalues.

IV. EQUIVALENCE METHOD OF CIG STATIONS IN THE ASYMMETRIC SYSTEM

A. Single-CIG Equivalence Method

In the asymmetric system, the equivalence method should be determined according to the coupling degree between the CIGs. Only when the CIGs are closely coupled with each other, will the system have only one pair of critical eigenvalues, and then the system can carry out the single-CIG equivalence. Fortunately, in most CIG stations, such as direct-drive wind farms and photovoltaic plants, the impedance of the collector line is small enough compared with the impedance of the grid. The coupling degree among all CIGs is close to 1. The critical eigenvalues of weak grid connected CIG stations are only one pair. Therefore, the CIG stations can be equivalent to one CIG.

1) Dynamic Parameters Identification of Equivalent CIG

In the CIG stations, all CIGs are closely coupled, and the voltages of CIGs are almost equal. Therefore, the voltages and phase angles of all CIGs are approximately equal. The sum of admittance of all CIGs is the detailed model of CIGs, which is of the $9n^{\text{th}}$ order. The equivalent model is the 9^{th} order. The expression of the equivalent model is known, which is the same as the CIG model in (1)–(2), and the parameters are to be determined according to the identification method. Finally, n CIGs are equivalent to one CIG, and the order of the dynamic model is reduced from $9n^{\text{th}}$ to 9^{th} .

To simulate a detailed CIG station with an equivalent CIG, it is only necessary to ensure that the admittance characteristics of the equivalent CIG and the detailed CIGs are consistent in the concerned frequency band. The parameters of equivalent CIGs can be solved by the least squares method. The objective function is:

$$\min F = \sum_{\omega=\omega_{\min}}^{\omega_{\max}} \left| Y_{\text{eq}}(j\omega) - \sum_{k=1}^n Y_k(j\omega) \right|^2 \quad (12)$$

where Y can be Y_{dd} , Y_{qq} , Y_{dq} or Y_{qd} respectively; the subscript eq represents equivalent model. Since there are four elements, the optimization objective is a multi-objective function, and can be converted to a single objective as follows:

$$\min F_{dd} + F_{qq} + F_{dq} + F_{qd} \quad (13)$$

Because the time scales of the inner-loop and outer-loop control of CIG are very different, these two parts should be identified separately. When identifying the outer-loop control parameters, the inner-loop transfer function is ignored, i.e., $G_{\text{ccd}}(s) = 1$, $G_{\text{ccq}}(s) = 1$, and the rest of the transfer functions are the same as (12). When identifying the inner-loop control parameters, the outer-loop control is ignored. The objective function is:

$$\min F = \sum_{\omega=\omega_{\min}}^{\omega_{\max}} \left| G_{\text{eq}}(j\omega) - \sum_{k=1}^n G_k(j\omega) \right|^2 \quad (14)$$

where G can be G_{ccd} or G_{ccq} to identify the PI parameters of the d -axis or q -axis current control respectively.

All PI control parameters can be obtained by identification. The main circuit parameters are calculated as follows:

$$\begin{aligned} L_{f,\text{eq}} &= 1 / \sum_{k=1}^n \frac{1}{L_{f,k}} \\ C_{\text{dc},\text{eq}} &= \sum_{k=1}^n C_{\text{dc},k} \\ v_{\text{dc}0,\text{eq}} &= \sum_{k=1}^n C_{\text{dc},k} v_{\text{dc}0,k} / \sum_{k=1}^n C_{\text{dc},k} \end{aligned} \quad (15)$$

2) Steady Parameters Calculation of Equivalent CIG Station

The power of the equivalent CIG is aggregated as follows:

$$P_{t,\text{eq}} = \sum_{i=1}^n P_{ti} \quad (16)$$

where n is the number of CIGs; P_t is the output power.

The equivalence of the CIG terminal transformer is regarded as a parallel connection. The impedance of transformer is:

$$Z_{T,\text{eq}} = 1 / \sum_{i=1}^n \frac{1}{Z_{Ti}} \quad (17)$$

According to the principle that the generalized short circuit ratio [22] of the system before and after equivalence is equal, the equivalent collector lines impedance is:

$$Z_{\text{col},\text{eq}} = Z_{\text{gscr}} - Z_g - Z_{T,\text{eq}} \quad (18)$$

where Z_{gscr} is the generalized short-circuit impedance of the CIGs, which is calculated according to [22]; Z_g is the system impedance as Fig. 2.

B. Multi-CIG Equivalence Method

When enhancing the damping of the system, the CIGs with stronger participation are usually selected as candidate locations to be controlled. Therefore, in the study of damping control, it would be better if the equivalent CIG model can distinguish the CIGs with different participations to critical eigenvalues. Obviously, the single-CIG equivalent model in the previous section cannot be used for this scenario. Therefore, the multi-CIG equivalence method is proposed in this section.

According to Section III.B.2, the participations of high PLL (or DVC) bandwidth CIGs and low PLL (or DVC) bandwidth CIGs to the critical eigenvalues are significantly different. Therefore, CIGs can be divided into two groups according to PLL bandwidth. Similarly, based on DVC bandwidth the CIGs can also be divided into two groups. Taking both into consideration, all the CIGs can be divided into four groups: low PLL bandwidth and low DVC bandwidth, low PLL bandwidth and high DVC bandwidth, high PLL bandwidth and low DVC bandwidth, high PLL bandwidth and high DVC bandwidth. The CIGs in each group adopt single-CIG equivalence. The parameters are calculated the same as the previous section.

The bandwidth boundaries of the high bandwidth group and the low bandwidth group are not invariant, but are determined according to the specific situation. This section gives the following method to divide the low and high bandwidth groups. The basic idea is that the CIGs ranking in the front several lower (the proportion is denoted as ζ) are in the low bandwidth group, and the remaining CIGs are in the high bandwidth group. The proportion ζ is determined according to the large sample data in the previous section. The method is as follows:

Step 1: Determine a constant k_η between 0 and 1, and obtain the bandwidth f_c . k_η is the proportion of the sum of the relative participation η of CIGs with less than f_c bandwidth to the relative participation η of the CIGs of whole samples. The relationship between k_η and f_c is as follows:

$$k_\eta(f_c) = \sum_{f \leq f_c} \eta(f) / \sum_{f \leq f_{\max}} \eta(f) \quad (19)$$

where η is relative participation, as shown in (9). k_η represents the participation of CIGs in the low bandwidth group to the critical eigenvalues. It is a determined according to experience,

which is taken as 0.5 in this paper. Given k_η , a f_c can be obtained.

Step 2: Calculate the proportion of all samples whose bandwidth is less than f_c to the whole samples, denoted as ζ , i.e.,

$$\zeta(f_c) = C(f \leq f_c) / C(f \leq f_{\max}) \quad (20)$$

where $C(f \leq f_c)$ is the number of samples whose bandwidth is less than f_c ; $C(f \leq f_{\max})$ is the number of whole samples. Given f_c , a ζ can be obtained.

Step 3: Sort all CIGs by bandwidth from lowest to highest, and divide the front ζ proportion CIGs in the low bandwidth group and the rest of the CIGs in the high bandwidth group. When there are n CIGs, the CIGs whose bandwidth is $\zeta \cdot n$ lower are the low bandwidth CIGs, and the rest are the high bandwidth CIGs.

Use Fig. 8 as an example. The dotted line intersects the horizontal axis at f_c . The proportion of the sum of η of the points on the left of the dotted line to the sum of η of all the points is k_η . The proportion of the number of points on the left of the dotted line to the total number of points is ζ .

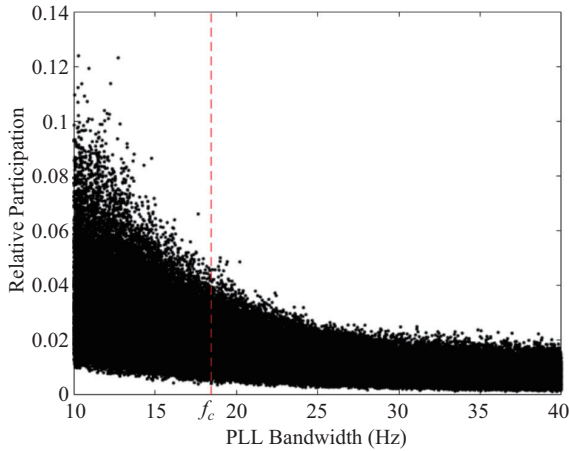


Fig. 8. Illustration diagram of PLL bandwidth.

The clustering results (select $k_\eta = 0.5$) are shown in Fig. 5. The two dotted lines on the xOy -plane represent the boundary between high and low bandwidth. These two lines divide all the CIGs into four groups. Basically, the CIGs with higher participation are grouped together, and the CIGs with lower participation are grouped into other groups.

The clustering method above is the only appropriate method. Other methods can be implemented according to the actual situation. Since the correlation between DVC bandwidth and relative participation is only a moderate correlation, the CIGs can be divided into two groups only considering the PLL bandwidth.

Theoretically, the more equivalent CIGs there are, the more accurate the model will be. But it will also be more complex. Compared with the detailed model, the multi-CIG equivalent model greatly reduces the system complexity. Compared with the single-CIG equivalence method, the multi-CIG equivalence method improves the accuracy, which is at the expense of complexity.

Furthermore, compared with the single-CIG equivalence method, the multi-CIG equivalence method has more abundant application scenarios. For example, when damping control is carried out, the CIGs with large participation are usually selected to exert control for better effect. There is only one CIG in the single-CIG equivalent model, which cannot distinguish those CIGs with large participation. However, the multi-CIG equivalence method can separate the CIGs with large participation and select the corresponding equivalent CIGs to apply the damping control.

V. SIMULATION

A. Small Signal Model of CIGs

The CIG station adopts the wind farm with a type IV wind turbine generator in this section. Its structure is an actual wind farm in Northwest, China. It includes 66 type IV wind turbine generators with rated power of 1.5 MW; it takes account of collector lines and CIG terminal transformers; and it is connected to a weak grid. This type IV wind turbine generator model is shown in Fig. 1. In the simulations, the wind farm adopts a small signal model, in which the wind turbine generators, lines and ground capacitances are all taken into account. The system state matrix (i.e., matrix A) is the 808th order.

$N = 2000$ sets of samples are randomly generated. In all samples, the coupling degree indexes between each CIG are calculated, and the average value coupling degree index is 0.9497. And there are only one pair of critical eigenvalues in all the samples. Although the wind turbine generators are not perfectly coupled (that is, $F \neq 1$), the coupling degree index is still much larger than 0.48, which is the result of the two-CIG system in Section III.D. Therefore, the wind turbine generators can be considered to be almost perfectly coupled, and the system have only one pair of critical eigenvalues. Fig. 9 shows a distribution of eigenvalues (solid dots), which is one of 2000 samples. It can be seen that there is only one pair of critical eigenvalues, although the wind turbine generators are not perfectly coupled.

The equivalent model of each sample is obtained by the proposed method. The accuracy of the equivalent models will be compared respectively.

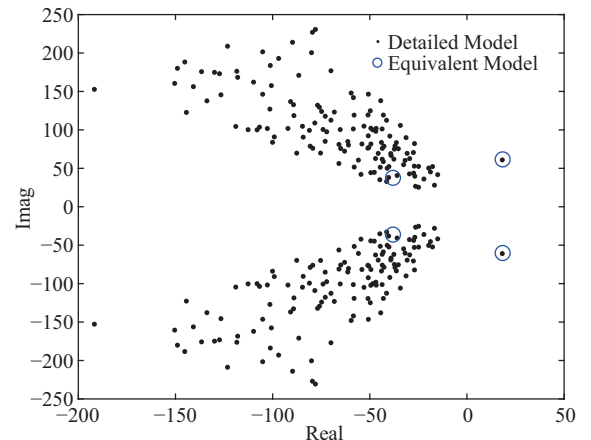


Fig. 9. Comparison of eigenvalues.

1) Accuracy Analysis of Single-CIG Equivalent Model

Using the sample in Fig. 9 as an example, draw the eigenvalues of its equivalent model in the same figure. It can be seen that the critical eigenvalues of the equivalent model are very close to those of the detailed model.

Critical eigenvalues of an equivalent wind farm and detailed wind farm are calculated respectively, and the error of critical eigenvalues will be obtained. After applying statistics, the histogram of the error distribution is shown in Fig. 10. The *x*-axis and *y*-axis are the real and imaginary parts of the errors of critical eigenvalues. The *z*-axis is the count of the errors of critical eigenvalues. It can be seen that the real part errors of the critical eigenvalues concentrate in the range of $-3\sim 2$ and the imaginary part errors concentrate in the range of $-3\sim 4$. The errors are all very small. The single-CIG equivalent model can approximately represent the detailed model.

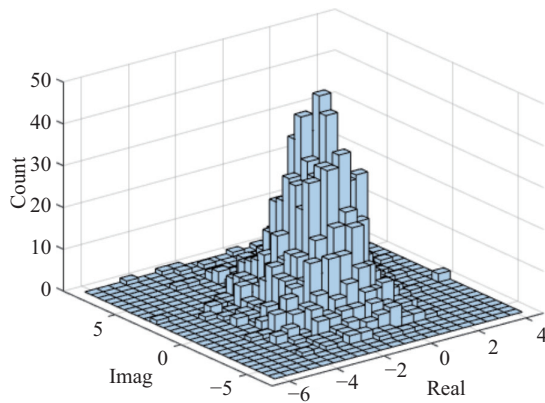


Fig. 10. Histogram of critical eigenvalue error of single-CIG equivalent model.

The statistical information of the errors of the real part, imaginary part, frequency, damping, amplitude and angle of the critical eigenvalues between the equivalent model and the detailed model is shown in Table V. It can be found that the errors of several indicators are relatively small and within the acceptable range.

TABLE V
COMPARISON OF CRITICAL EIGENVALUES ERROR

Indicators	Mean	Standard deviation
Real part	-0.7524	1.1129
Imaginary part	0.4955	1.9917
Frequency	0.0789	0.3170
Damping	0.0127	0.0179
Amplitude	0.1217	1.8983
Angle	0.8107	1.1410

2) Accuracy Analysis of Multi-CIG Equivalent Model

For critical eigenvalues, such as the previous section, the histogram of error distribution is shown in Fig. 11. The *x*-axis and *y*-axis are the real and imaginary parts of the errors of critical eigenvalues. The *z*-axis is the count of the errors of critical eigenvalues. It is shown that the real part errors of the critical eigenvalues are almost within $-2\sim 1$ and the imaginary part errors are almost within $-2\sim 3$. The multi-CIG equivalent model can also approximately represent the detailed model.

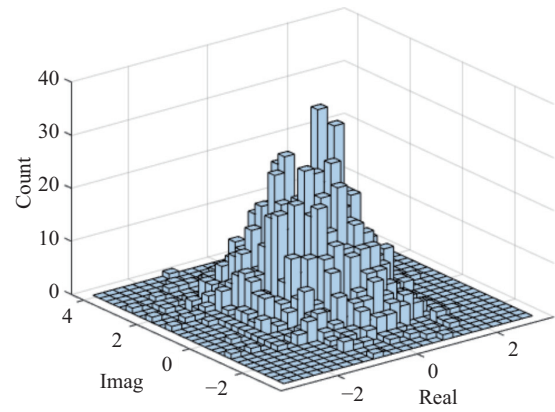


Fig. 11. Histogram of critical eigenvalue error of multi-CIG equivalent model.

The relative participation of each equivalent CIG to the critical eigenvalues is calculated, and is compared with the sum of the relative participation of the detailed CIGs. The statistical information of errors of the relative participation of the four equivalent CIGs is shown in Table VI. It can be seen that the relative participation errors of each equivalent CIG are all small, which can better reflect the participation of the detailed CIGs to the critical eigenvalues. According to the equivalence method, the CIGs in group 1 has the greatest participation. If damping control is applied, a better candidate location could be equivalent CIG 1.

TABLE VI
COMPARISON OF RELATIVE PARTICIPATION ERROR

Indicators	Mean ($\times 10^{-2}$)	Standard deviation ($\times 10^{-2}$)
Equivalent CIG 1	0.0633	1.1188
Equivalent CIG 2	0.4295	1.2134
Equivalent CIG 3	-0.3538	0.6268
Equivalent CIG 4	-0.1390	0.8059

The state matrix of the multi-CIG equivalent model is reduced from the 808th to 56th order compared with that of the detailed model which is greatly reduced in complexity. Compared with the single-CIG equivalent model, it can be clearly seen that the error of the multi-CIG equivalent model is much smaller as shown in Figs. 10 and 11. Furthermore, the relative participation of each equivalent CIG to the critical eigenvalues can better reflect the participation of the detailed CIGs, which the single-CIG equivalent model cannot do.

B. Electromagnetic Transient Model of CIGs

In this section, the electromagnetic transient simulation is to prove the accuracy of the equivalent model in a nonlinear simulation. The accuracy is evaluated by whether the oscillation waveforms in the detailed model and equivalent model is consistent in the studied time scale. The waveforms of the active power of the wind farm and the DC voltage of the wind turbine generator are selected, since both theoretical and practical observations show that when the wind farm with type IV wind turbine generators oscillates, these two variables can both observe the oscillation mode. In order to excite the oscillation mode, a three-phase instantaneous short-circuit fault is applied at the outgoing line.

Electromagnetic transient simulation software, such as PSCAD, can hardly simulate a large-scale system. Therefore, a simple wind farm model, which contains 4 type IV wind turbine generators, is established on PSCAD. The parameters of the CIG bandwidths are shown in Table VII. The multi-CIG equivalent model contains two CIGs. CIG 1 and 2 are in group 1, and CIG 1 and 2 are in group 2.

The three-phase instantaneous fault is set on the transmission line at 0.1 s, which lasts 20 ms. The active power and DC voltage after the fault in the detailed and equivalent wind farm are observed respectively, which are shown in Fig. 12. The DC voltage belongs to CIG 1 in the detailed model, and equivalent CIG 1 in the multi-CIG equivalent model respectively. As can be seen from Fig. 12, no matter whether it is from the wind farm active power or the CIG DC voltage, the equivalent models are both close to the detailed model. The equivalent models can reflect the oscillation mode of the system.

TABLE VII
PARAMETERS OF CIGS BANDWIDTH

CIG	PLL bandwidth (Hz)	DVC bandwidth (Hz)
CIG 1	10	13
CIG 2	15	10
CIG 3	20	21
CIG 4	25	17

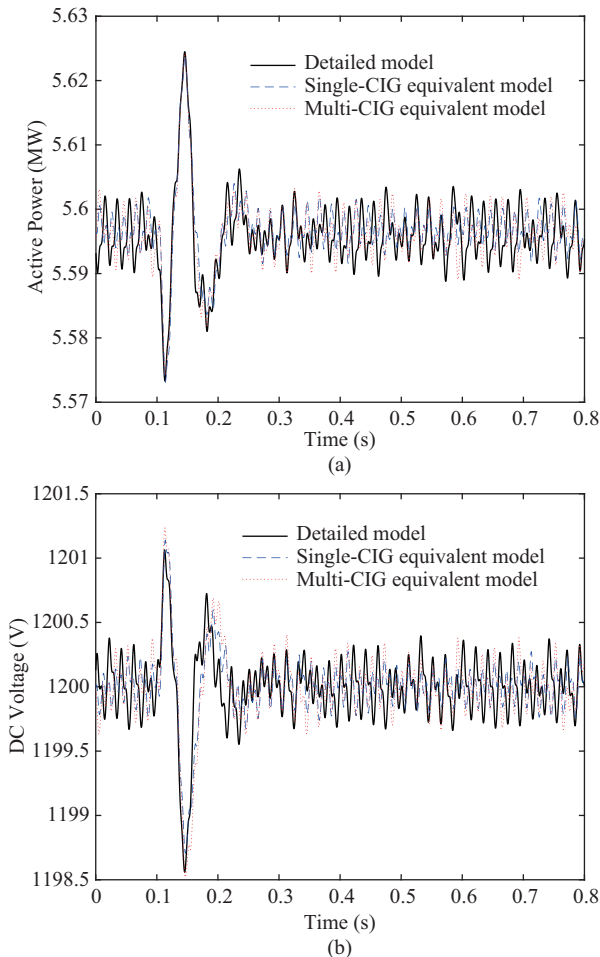


Fig. 12. Time domain simulation curves comparison. (a) Active power. (b) DC Voltage.

VI. CONCLUSION

In this paper, the oscillation characteristics of multiple weak grid connected converter interfaced generations (CIGs) with different parameters are studied based on large samples of the Monte Carlo simulation. The single-CIG and multi-CIG dynamic equivalence methods in stations with multiple CIGs are proposed respectively. The conclusions are as follows:

1) The number of critical eigenvalues and the participation of each CIG to the critical eigenvalues are related to the coupling degree of CIGs. When the CIGs are perfectly coupled, the system has only one pair of critical eigenvalues. The participation of each CIG to the critical eigenvalues is strongly negative correlated with a phase locked loop (PLL) bandwidth, moderate negative correlated with a DC voltage control (DVC) bandwidth, and basically irrelevant with other parameters. As the coupling degree of CIGs decreases, the number of critical eigenvalues increases and the participations of all CIGs also changes. Particularly, when n CIGs are perfectly decoupled, the system has n pairs of critical eigenvalues, and only one CIG participates in the pair of critical eigenvalues.

2) In the system of multiple weak grid connected CIGs, when CIGs are closely coupled with each other, there is only one pair of critical eigenvalues and the single-CIG equivalence can be carried out. And CIGs in most real stations are closely coupled. Therefore, this paper proposes a single-CIG equivalence method. The equivalent CIG parameters are identified based on the consistency of the output admittance characteristics. Simulation results under large samples show that the critical eigenvalues errors before and after equivalence are very small. The equivalent model is simple and can be used to analyze the system stability.

3) In order to apply damping control better, it is necessary to further determine the candidate location based on the participation of the CIGs. Therefore, a multi-CIG equivalence method is proposed. According to the participation of each CIG to the critical eigenvalues, the station is equivalent to a multi-CIG model. This method first classifies the CIGs into several groups based on PLL bandwidth and DVC bandwidth, and then carries out the single-CIG equivalence in each group. A large number of simulations shows that the equivalent model can reflect the participation of CIGs in the detailed model to the critical eigenvalues. Moreover, the error of critical eigenvalues is lower than the single-CIG equivalent model. The equivalent model is more complex, and could be used to study damping control.

REFERENCES

- [1] N. Hatziaargyriou, J. V. Milanović, C. Rahmann, V. Ajarapu, C. Canizares, I. Erlich, D. Hill, I. Hiskens, I. Kamwa, B. Pal, P. Pourbeik, J. Sanchez-Gasca, A. Stankovic, T. V. Cutsem, V. Vittal, and C. Vournas, "Definition and classification of power system stability-revisited & extended," *IEEE Transactions on Power Systems*, vol. 36, no. 4, pp. 3271–3281, Jul. 2021.
- [2] L. S. Xiong, X. K. Liu, Y. H. Liu, and F. Zhuo, "Modeling and Stability Issues of Voltage-source Converter-dominated Power Systems: A Review," *CSEE Journal of Power and Energy Systems*, vol. 8, no. 6, pp. 1530–1549, Nov. 2022.

- [3] Y. Z. Cheng, L. L. Fan, J. Rose, J. Schmall, F. Huang, J. R. Ramamurthy, A. Mulawarman, P. G. Mysore, Z. X. Miao, Y. Li, Y. K. Xu, M. Zhang, S. Shah, P. Koralewicz, R. Wallen, V. Gevorgian, F. Salehi, M. Tabrizi, W. J. Lee, X. R. Xie, A. Issac, A. Dissanayaka, P. Zadhkash, D. Howard, L. Xu, M. Lwin, A. Goharrizi, B. Pal, H. R. Ali, L. Kunjumammed, J. Sun, Y. F. Gong, U. Karaagac, J. Mahseredjian, I. Kocar, A. Trevisan, H. Gras, and R. Gagnon, "Wind energy systems sub-synchronous oscillations: events and modeling," *IEEE Power & Energy Society, PES-TR80*, pp. 1–3, Jul. 2020.
- [4] Y. H. Huang, X. M. Yuan, J. B. Hu, and P. Zhou, "Modeling of VSC connected to weak grid for stability analysis of DC-link voltage control," *IEEE Journal of Emerging and Selected Topics in Power Electronics*, vol. 3, no. 4, pp. 1193–1204, Dec. 2015.
- [5] D. Wang, L. Liang, L. Shi, J. B. Hu, and Y. H. Hou, "Analysis of modal resonance between PLL and DC-link voltage control in weak-grid tied VSCs," *IEEE Transactions on Power Systems*, vol. 34, no. 2, pp. 1127–1138, Mar. 2019.
- [6] X. F. Wang, L. Harnefors, and F. Blaabjerg, "Unified impedance model of grid-connected voltage-source converters," *IEEE Transactions on Power Electronics*, vol. 33, no. 2, pp. 1775–1787, Feb. 2018.
- [7] H. K. Liu, X. R. Xie, J. B. He, T. Xu, Z. Yu, C. Wang, and C. Y. Zhang, "Subsynchronous interaction between direct-drive PMSG based wind farms and weak AC networks," *IEEE Transactions on Power Systems*, vol. 32, no. 6, pp. 4708–4720, Nov. 2017.
- [8] W. S. Wang, C. Zhang, G. Q. He, G. H. Li, J. Y. Zhang, and H. J. Wang, "Overview of research on subsynchronous oscillations in large-scale wind farm integrated system," *Power System Technology*, vol. 41, no. 4, pp. 1050–1060, Apr. 2017.
- [9] R. T. H. Alden, P. J. Nolan, and J. P. Bayne, "Shaft dynamics in closely coupled identical generators," *IEEE Transactions on Power Apparatus and Systems*, vol. 96, no. 3, pp. 721–728, May 1977.
- [10] X. T. Wang and F. Yang, "Equivalent simplification of torsional dynamics in the closely coupled identical turbine-generators," in *2006 IEEE Power Engineering Society General Meeting*, Montreal, QC, Canada, 2006, pp. 1–4.
- [11] G. G. Yan, D. Wang, Q. Jia, and W. B. Hu, "Equivalent modeling of DFIG-based wind farms for sub-synchronous resonance analysis," *Energies*, vol. 13, no. 20, pp. 5426, Oct. 2020.
- [12] W. J. Du, W. K. Dong, H. F. Wang, and J. Cao, "Dynamic aggregation of same wind turbine generators in parallel connection for studying oscillation stability of a wind farm," *IEEE Transactions on Power Systems*, vol. 34, no. 6, pp. 4694–4705, Nov. 2019.
- [13] J. L. Agorreta, M. Borrega, J. López, and L. Marroyo, "Modeling and control of n -paralleled grid-connected inverters with LCL filter coupled due to grid impedance in PV plants," *IEEE Transactions on Power Electronics*, vol. 26, no. 3, pp. 770–785, Mar. 2011.
- [14] S. H. Liao, M. Huang, X. M. Zha, and J. M. Guerrero, "Emulation of multi-inverter integrated weak grid via interaction-preserved aggregation," *IEEE Journal of Emerging and Selected Topics in Power Electronics*, vol. 9, no. 4, pp. 4153–4164, Aug. 2021.
- [15] W. Dong, H. H. Xin, D. Wu, and L. B. Huang, "Small signal stability analysis of multi-infeed power electronic systems based on grid strength assessment," *IEEE Transactions on Power Systems*, vol. 34, no. 2, pp. 1393–1403, Mar. 2019.
- [16] W. J. Du, W. K. Dong, and H. F. Wang, "A method of reduced-order modal computation for planning grid connection of a large-scale wind farm," *IEEE Transactions on Sustainable Energy*, vol. 11, no. 3, pp. 1185–1198, Jul. 2020.
- [17] C. Chen, W. J. Du, L. A. Wang, and H. F. Wang, "Mechanism investigation of sub-synchronous oscillations in power systems as caused by multi-modal resonance within DFIG-based wind farm," *Proceedings of the CSEE*, vol. 39, no. 3, pp. 642–651, Feb. 2019.
- [18] Y. H. Huang, D. Wang, L. Shang, G. R. Zhu, H. Y. Tang, and Y. Li, "Modeling and stability analysis of DC-link voltage control in multi-VSCs with integrated to weak grid," *IEEE Transactions on Energy Conversion*, vol. 32, no. 3, pp. 1127–1138, May 2017.
- [19] M. Q. Zhang, X. M. Yuan, and J. B. Hu, "Path series expansion method based on self-/En-stabilizing properties and its application in the stability analysis of power systems with diversified power electronic devices," *Proceedings of the CSEE*, vol. 41, no. 5, pp. 1637–1654, Mar. 2021.
- [20] W. C. Zhai, Q. Jia, and G. G. Yan, "Analysis of sub synchronous oscillation characteristics from a direct drive wind farm based on the complex torque coefficient method," *CSEE Journal of Power and Energy Systems*, doi: 10.17775/CSEEJPES.2021.05760.
- [21] S. H. Liao, X. M. Zha, X. Z. Li, M. Huang, J. J. Sun, J. Pan, and J. M. Guerrero, "A novel dynamic aggregation modeling method of grid-connected inverters: application in small-signal analysis," *IEEE Transactions on Sustainable Energy*, vol. 10, no. 3, pp. 1554–1564, Jul. 2019.
- [22] H. H. Xin, D. Q. Gan, and P. Ju, "Generalized short circuit ratio of power systems with multiple power electronic devices: analysis for various renewable power generations," *Proceedings of the CSEE*, vol. 40, no. 17, pp. 5516–5526, Sep. 2020.
- [23] M. Liserre, R. Cárdenas, M. Molinas, and J. Rodríguez, "Overview of multi-MW wind turbines and wind parks," *IEEE Transactions on Industrial Electronics*, vol. 58, no. 4, pp. 1081–1095, Apr. 2011.
- [24] M. Waseem, Y. H. Feng, Y. N. Qiu, C. Sun, and H. A. Sher, "Improved vector current control for grid side converter in PMSG wind turbine with fault tolerance capability," in *8th Renewable Power Generation Conference (RPG 2019)*, Shanghai, China, 2019, pp. 1–8.
- [25] F. Dorfler and F. Bullo, "Kron reduction of graphs with applications to electrical networks," *IEEE Transactions on Circuits and Systems I: Regular Papers*, vol. 60, no. 1, pp. 150–163, Jan. 2013.
- [26] CIGRE Working Group B4.41, *Systems with Multiple DC Infeed*, Paris: CIGRE Working Group B4.41, pp. 16–17, Dec. 2008.
- [27] Y. Shao and Y. Tang, "Fast evaluation of commutation failure risk in multi-infeed HVDC systems," *IEEE Transactions on Power Systems*, vol. 33, no. 1, pp. 648–653, Jan. 2018.
- [28] L. B. Huang, H. H. Xin, Z. Y. Li, P. Ju, H. Yuan, and G. Z. Wang, "Identification of generalized short-circuit ratio for on-line stability monitoring of wind farms," *IEEE Transactions on Power Systems*, vol. 35, no. 4, pp. 3282–3285, Jul. 2020.
- [29] J. Beerten, S. D'Arco and J. A. Suul, "Identification and small-signal analysis of interaction modes in VSC MTDC systems," *IEEE Transactions on Power Delivery*, vol. 31, no. 2, pp. 888–897, Apr. 2016.



Longyuan Li received B.S. and Ph.D. degrees in Electrical Engineering from Southwest Jiaotong University, Chengdu, China, in 2012 and 2022, respectively. His research interests include wind power modeling and power system stability analysis with large-scale wind power integration.



Ruiqing Fu received a B.S. degree in Electrical Engineering from Hebei University of Science and Technology, Hebei, China, in 2012, an M.S. degree in Electrical Engineering from Beijing Jiaotong University, Beijing, China, in 2015. He is currently pursuing a Ph.D. degree at Southwest Jiaotong University, Sichuan, China. His research interests include stability analysis and control of power system with wind power integration.



Xiaoqin Lyu received M.S. and Ph.D. degrees in Electrical Engineering from Southwest Jiaotong University, Chengdu, China, in 2006, and 2020 respectively. Since 2013, she has been an Associate Professor in the School of Electrical Engineering, Southwest Jiaotong University. Her main research interests are the power quality, modeling and stability analysis of the electrical railway traction network and electrical rail vehicle systems.



Xiaoru Wang received B.S. and M.S. degrees from Chongqing University, China, in 1983 and 1988, respectively, and a Ph.D. degree from Southwest Jiaotong University, China, in 1998. Since 2002, she has been a Professor in the School of Electrical Engineering, Southwest Jiaotong University. Her main research interests are electric power systems protection and stability control, integrated renewable energy and smart grid.